Wang *et al.*
Chinese Journal of Mechanical Engineering (2022) 35:136
https://doi.org/10.1186/s10033-022-00809-x

Chinese Journal of Mechanical Engineering

ORIGINAL ARTICLE

Open Access

Development and Control of a Magnetorheological Damper-Based Brake Pedal Simulator for Vehicle Brake-by-Wire Systems

Daoming Wang[1*], Biao Wang[1], Bin Zi[1], Xianxu Bai[2] and Wuwei Chen[2]

Abstract

Recent developments have demonstrated that the brake pedal simulator (BPS) is becoming an indispensable apparatus for the break-by-wire systems in future electric vehicles. Its main function is to provide the driver with a comfortable pedal feel to improve braking safety and comfort. This paper presents the development and control of an adjustable BPS, using a disk-type magnetorheological (MR) damper as the passive braking reaction generator to simulate the traditional pedal feel. A detailed description of the mechanical design of the MR damper-based BSP (MRDBBPS) is presented in this paper. Several basic performance experiments on the MRDBBPS prototype are conducted. A return-to-zero (RTZ) algorithm is proposed to avoid hysteresis and improve the repeatability of the pedal force. In addition, an RTZ algorithm-based real-time current-tracking controller (RTZRC) is designed in consideration of the response lag of the coil circuit. Finally, an experimental system is established by integrating the MRDBBPS prototype into a self-developed automotive MR braking test bench (AMRBTB), and several control and braking experiments are performed. This research proposes a RTZRC control algorithm which can significantly increase the tracking accuracy of the brake pedal characteristic curve, particularly at a high pedal velocity. Additionally, the designed MRDBBPS prototype can achieve an effective and favorable control of the AMRBTB with a good repeatability.

Keywords: Brake pedal simulator, Magnetorheological damper, Return-to-zero algorithm, Real-time current-tracking control, Experimental evaluation

1 Introduction

As vehicles develop towards electrification, intellectualization, lightweightness, and integration [1], the disadvantages such as complex structure, low efficiency, and response lag of the conventional hydraulic braking (CHB) system are becoming increasingly prominent. The brake-by-wire (BBW) system, characterized by high efficiency, energy-saving, fast response, and flexible layout, is becoming the development trend of the future electric vehicle braking systems [2, 3]. It uses an electronically controlled brake actuator to achieve vehicle braking without a direct mechanical or hydraulic connection between the brake actuator on each wheel and the brake pedal [4–6]. Here, the driver cannot directly perceive the braking reaction fed back to the brake pedal during vehicle braking, which means the traditional brake pedal feel (BPF) is lost. Therefore, a new type of brake pedal simulator (BPS) suitable for the BBW system should be developed. By accurately simulating the traditional pedal characteristics between the pedal force and pedal displacement, a comfortable BPF can be supplied for the driver to improve braking safety and comfort [7].

*Correspondence: cumtcmeewdm@hotmail.com

[1] School of Mechanical Engineering, Hefei University of Technology, Hefei 230009, China
Full list of author information is available at the end of the article

There are generally two types of BPS: non-adjustable and adjustable. The non-adjustable BPS can only simulate a fixed relation curve between the pedal force and pedal displacement. Aoki et al. [8] designed a BPS consisting of rubbers, cylinders, and springs. The BPF is generated via the compression of the rubbers. Zehnder et al. [9] developed a BPS based on rubber and coil springs. The rubber spring is used to simulate the BPF and the coil spring is used for the automatic return of the brake pedal. The pedal force of the BPS is limited to be less than 200 N. Liu et al. [10] proposed a BPS consisting of two inline springs and a parallel spring for application in the electrohydraulic hybrid braking system. Yu et al. [11] designed a BPS using two torsion springs to simulate the BPF and pushed the pedal back in situ when released. The adjustable BPS is superior to the non-adjustable one in terms of better adjustability and adaptability. It can simulate the alterable pedal characteristics to produce the desired BPF for the driver. Flad et al. [12] designed an adjustable BPS that was primarily composed of a stepper motor, planetary gear, and brake pedal. It could simulate the required pedal characteristics online by regulating the resistance torque of the step motor. Farshizadeh et al. [13] presented the design of a BPS using a motor and rack-pinion mechanism to produce the braking reaction. Hildebrandt et al. [14] developed a BPS by combining an electric pump, a servo valve, and a differential cylinder.

In summary, although the non-adjustable BPS is simple in structure, it cannot satisfy the differentiated requirements of the desired BPF among various types of vehicles and drivers of different genders, ages, and driving experiences. For the adjustable type, electric motors and pumps are generally used to provide the braking reaction. However, this may generate discomfort to drivers because of their rigidity property in nature. Additionally, they are frequently bulky and heavy, which is not conducive to the lightweightness and integration of the vehicle braking system. Consequently, a soft, compact yet powerful, and passive damping device is required to produce a comfortable BPF for the BPS.

Over the past decades, the emergence of smart materials has significantly accelerated the development of engineering equipment. Magnetorheological fluids (MRFs) belong to the family of smart materials, typically containing micro-sized ferromagnetic particles suspended in carrier fluids [15–18]. They have been widely applied in the vehicle industry [19], such as in suspensions [20–22], shock absorbers [23, 24], clutches [25], and brakes [26, 27], owing to their outstanding rheological properties. The magnetorheological (MR) damper employs MRFs as the operating media to produce a controllable damping force accurately, efficiently, and conveniently solely by adjusting the coil current. Compared with conventional active power components, it has the advantages of a large torque/weight ratio, low power consumption, rapid response, and better controllability [28]. In many applications involving rehabilitation robots [28, 29], haptic gloves [30], teleoperation [31], medical [32], and virtual reality [33], the MR damper has proved to be a suitable option for passive-force-generation devices.

In addition, the accurate simulation of BPS has important reference value for driver braking judgment. Day et al. [34] simulated the parameters that affected BPS in AMESim simulation software, and got a good brake pedal feel. A new hybrid genetic neural network optimization model has been proposed and applied to the dynamic control and optimization of braking performance and brake pedal stroke in the braking process [35]. Yan et al. [36] studied the application of model predictive control schemes and robust H_∞ state feedback control in trajectory tracking, and tested the performance of control algorithms under different conditions. The BPS is established in Matlab/Simulink software, and a detailed mathematical description of the vacuum booster system is carried out [37]. All these provide the basis for the best BPS control.

This study aims to develop an adjustable BPS to simulate the traditional BPF for the vehicle BBW system. For this, a disk-type MR damper is designed as the generator of the passive braking reaction under the excitation of a low-voltage direct current. Since the BPF is described by the relationship curve between pedal displacement and pedal force, known as the brake pedal characteristic curve (BPCC), a precise real-time tracking control of the BPCC is still necessary for the BPS to provide the driver with an accurate and comfortable BPF. Therefore, a return-to-zero (RTZ) algorithm is proposed to avoid the inherent magnetic hysteresis associated with the MR damper. In addition, a real-time current-tracking controller integrated with the RTZ algorithm is designed in consideration of the response lag of the coil circuit. The control effect of the proposed current-tracking algorithm and the practical application performance of the MR damper-based BPS (MRDBBPS) prototype are evaluated through experiments.

The highlight of this paper is that a controllable magnetorheological damper with compact structure and continuous damping force is designed to simulate the pedal force, and a current tracking controller based on RTZ algorithm is proposed, which effectively improves the simulation effect of the pedal force. Finally, a MRDBBPS prototype is built and braking experiments are carried out with AMRBTB to verify that the designed MRDBBPS prototype can effectively control AMRBTB. Compared with other adjustable BPS based on motor and pump, the MRDBBPS designed in this study can adjust the pedal

feeling according to personal habit vehicle performance, and can simply and quickly meet people's individual needs. In addition, its mechanical structure is relatively simple, which is more conducive to the integrated design of electric vehicles in the future [38].

The remainder of this paper is structured as follows: the mechanical design and basic performance experiments of the MRDBBPS are described in Section 2. Section 3 presents the design and implementation of a real-time current-tracking control algorithm for the accurate simulation of the BPCC. Section 4 describes the development of an automotive MR braking system integrating with the MRDBBPS prototype, and the experimental evaluation of the control effect of the current-tracking algorithm and the practical application performance of the MRDBBPS prototype. Finally, the paper is concluded in Section 5.

2 Development of the MRDBBPS

Figure 1 shows the configuration of the proposed MRDBBPS. An encoder is connected to the pedal shaft through an elastic coupling, and a pedal force sensor is fixed on the brake pedal. Two ends of a torsion spring are connected with the brake pedal and support, respectively. An overrunning clutch is used to achieve the power engagement/disengagement between the pedal shaft and driving gear. The driven gear is connected to the MR damper. During the process of vehicle braking, the pedal force sensor detects the pedal force, and the encoder obtains both the pedal displacement and pedal velocity when the driver steps on the pedal. The collected signals are transmitted to a data acquisition and control unit that is also used as the current supply for the MR damper to generate the required damping force. During this period, the driver perceives the braking reaction, known as BPF.

In contrast, the overrunning clutch separates the pedal shaft from the driving gear when the driver releases the pedal, and the brake pedal automatically resets under the action of the torsion spring.

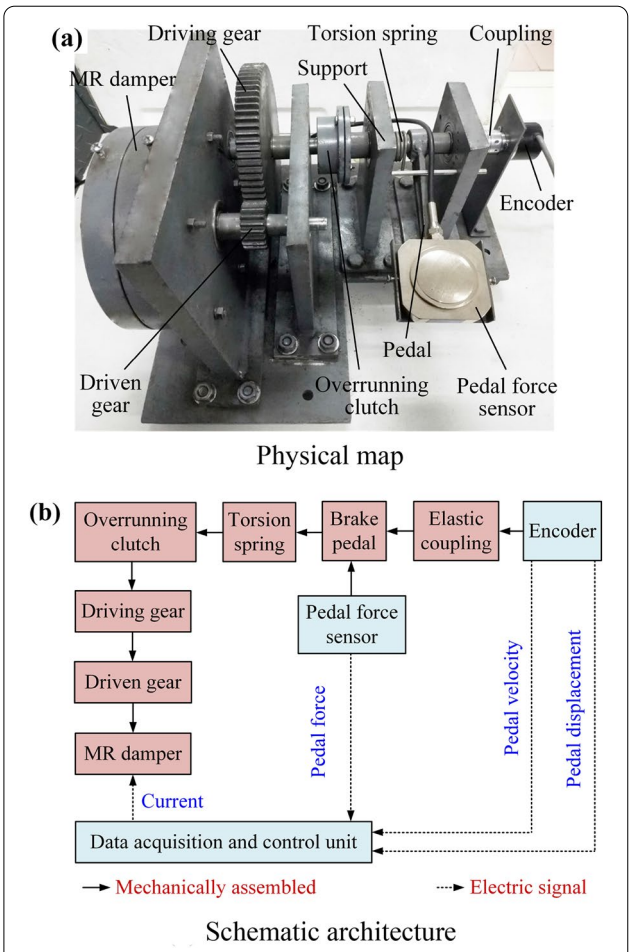

Figure 1 Configuration of the proposed MRDBBPS

2.1 Performance Index Requirements

Performance indexes of the designed MRDBBPS are listed as follows: the maximum pedal displacement was 120 mm, the maximum pedal force was 500 N, and the maximum pedal velocity is 500 mm/s. Figure 2 shows the force diagram of the brake pedal. In the figure, P_1 represents the initial position of the pedal, and P_2 is the position after the pedal rotates at an angle of α. F is the pedal force, and r is the vertical distance from the action center of the pedal force to the rotational centerline of the pedal shaft. In the design, $r = 150$ mm.

In the preliminary design, without considering the spring force and friction resistance, the relationship between the pedal force F and the damping torque of the MR damper T_M, and that between the pedal velocity v and the rotational speed of the driven gear n are described by

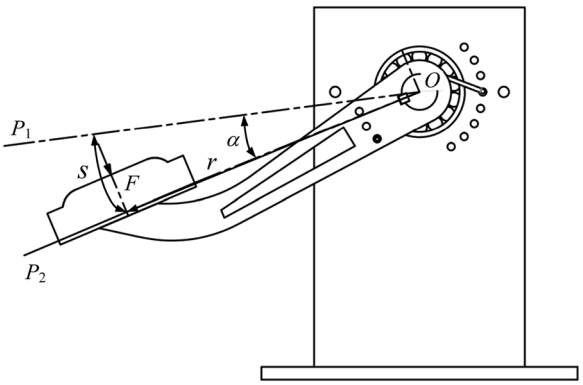

Figure 2 Force diagram of the brake pedal

$$T_{\mathrm{M}} = \frac{r}{i} \cdot F, \tag{1}$$

$$n = \frac{30i}{\pi r} \cdot v, \tag{2}$$

where i is the transmission ratio of the driving gear and driven gear; $i = 4$. By substituting the values of the performance indexes and i into Eqs. (1), (2), the required maximum damping torque of the MR damper is calculated as $\mathrm{T}_{\mathrm{M_{max}}} = 18.75\ \mathrm{N \cdot m}$, the maximum rotational speed of the driven gear is $n_{\max} = 127$ r/min, and the maximum rotation angle of the pedal is 45.84°.

2.2 Design of the Disk-Type MR Damper

As described above, a disk-type MR damper shown in Figure 3 is designed to provide the braking reaction for the BPS. Without current supplied to the coil, the MRFs, filled in the working gap between the disk and the housing, exhibits Newtonian fluid characteristics, resulting in a very small damping torque. When the coil is energized, a magnetic field is generated in the working gap. The ferromagnetic particles in the MRFs attract to form a solid-like structure perpendicular to the disk instantly, and a large damping torque is produced. In this design, a single-disk form is utilized for the MR damper. According to Ref. [28], the total damping torque T_{M} can be expressed as

$$T_{\mathrm{M}} = \frac{4}{3}\pi\tau_y(R_2^3 - R_1^3) + \frac{\pi\eta\omega}{h}(R_2^4 - R_1^4), \tag{3}$$

where τ_y is the field-induced shear stress of the MRFs, η is the apparent viscosity of the MRFs, R_2 and R_1 are the effective outer and inner radii of the working gap, respectively, h is the working gap thickness, and ω is the angular velocity of the shaft; $\omega = n\pi/30$.

The material properties of the MRFs significantly affect the operating performance of the MR damper. In this study, a type of MRFs (model SG-MRF2035), provided by Ningbo Shangong Monitoring and Control Engineering Co., Ltd., is selected. Its apparent viscosity is $\eta = 240\ \mathrm{MPa \cdot s}$. Referring to the relationship between the field-induced shear stress τ_y and the magnetic flux density B measured in our previous study [39], the following equation is derived using the polynomial fitting method

$$\begin{aligned}\tau_y = &-0.84034 + 57.88768B + 126.059485B^2 \\ &-216.76608B^3 + 85.27012B^4.\end{aligned} \tag{4}$$

Eq. (4) indicates that τ_y is fully determined by B. For a coil current of 1.1 A, a two-dimensional electromagnetic simulation of the MR damper is conducted. The distribution of magnetic flux density is shown in Figure 4,

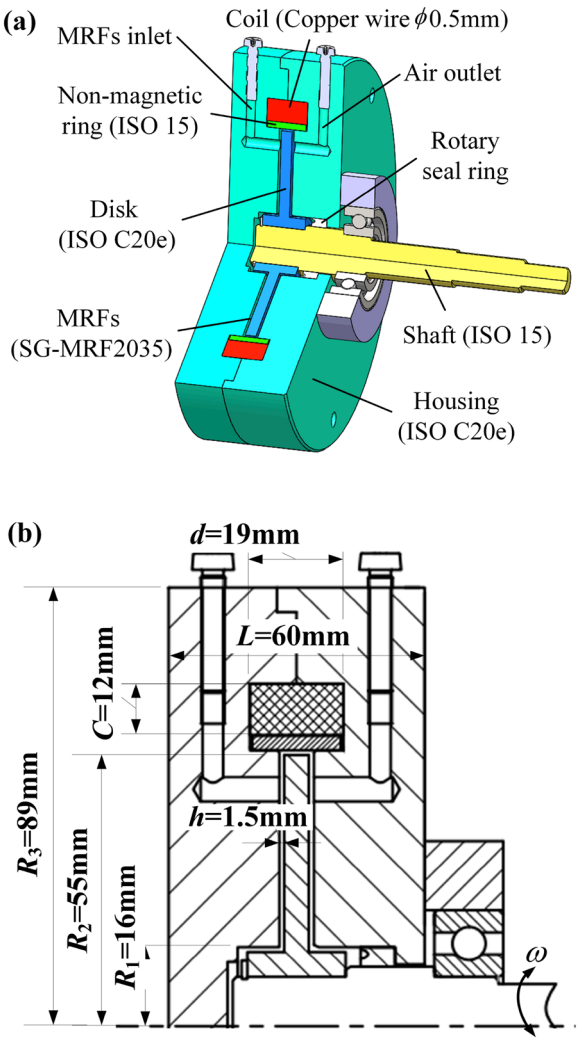

Figure 3 Structural diagram of the disk-type MR damper: (**a**) Three-dimensional model, (**b**) two-dimensional sectional view

which shows that the maximum flux density appears at the housing near the coil and its value is approximately 1.57 T, which is lower than the saturation flux density of the selected material (ISO C20e). Moreover, the flux density distributes approximately uniformly along the radial direction of the working gap with an average value of 0.44 T. Combining Eqs. (1) to (4), the total damping torque is calculated as $T_{\mathrm{M}} = 22.9\ \mathrm{N \cdot m} > \mathrm{T}_{\mathrm{M_{max}}} = 18.75\ \mathrm{N \cdot m}$, which means the torque output of the MR damper satisfies the design requirements.

2.3 Selection of the Torsion Spring

As mentioned earlier, the main function of the torsion spring is to provide a reaction force to the pedal when

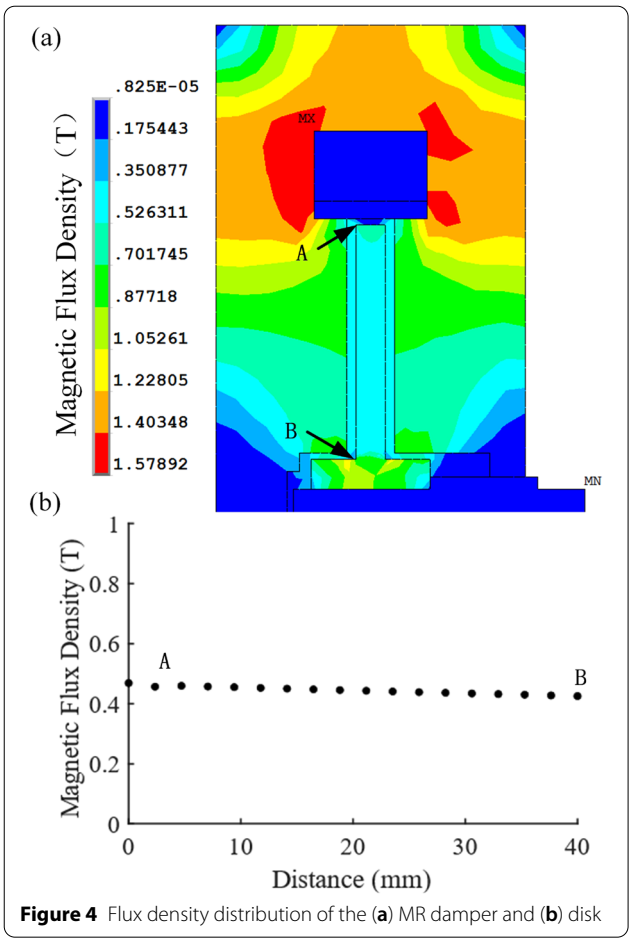

Figure 4 Flux density distribution of the (**a**) MR damper and (**b**) disk

released. However, while the pedal is pressed, the torsion spring also produces a resistance expressed as

$$T_s = \frac{Ed_s^4\alpha_s}{3670nD_s}, \tag{5}$$

where T_s is torsional resistance torque of the torsion spring; E is the elastic modulus of the material for the torsion spring, E=206 GPa; d_s is the wire diameter, d_s=3 mm; D_s is the mean diameter of the torsion spring, D_s=29 mm; n is the effective number of the wire turns, n=4; and α_s the torsional angle of the spring.

By substituting the above parameter values into Eq. (5), T_s can be rewritten as

$$T_s = 0.0392\alpha_s. \tag{6}$$

According to Figure 2, the relationship between the pedal displacement s and the torsional angle of the spring α_s is expressed as

$$s = \frac{\alpha_s}{180}r\pi. \tag{7}$$

Thus, the relationship between T_s and s can be written as

$$T_s = 0.015s. \tag{8}$$

The maximum torsional resistance torque provided by the torque spring is calculated as 1.8 N·m by substituting the value of maximum pedal displacement into Eq. (8). It accounts for approximately 7.8% of the total damping force of the MR damper; thus it is ignored in this study.

2.4 Basic Performance Experiments

Without coil current applied to the MR damper, the pedal force is the sum of the Coulomb friction resistance generated by bearings and rotary rings and the viscous resistance of the MRFs. It is measured at different pedal velocities and the results are plotted in Figure 5(a). As observed, the value of the pedal force is considerably small, basically fluctuating at approximately around 16 N. Figure 5(b) presents the variation in the pedal force with time for a coil current of 0.4 A. The pedal force is observed to increase slightly with the pedal velocity,

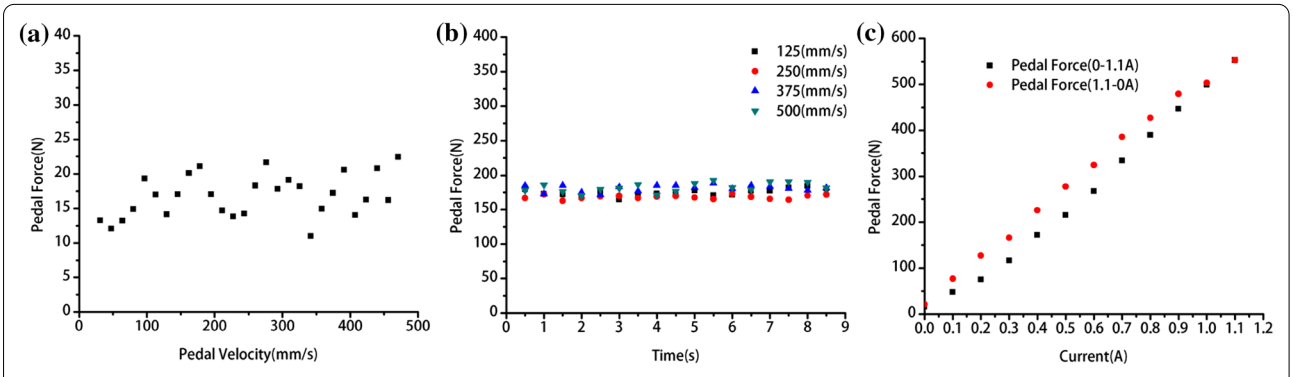

Figure 5 Experimental results of basic performances for the MRDBBPS prototype: (**a**) Pedal force versus pedal velocity (I = 0 A), (**b**) pedal forces at different pedal velocities, (**c**) pedal force versus coil current for the current increasing and decreasing stages

which means that the pedal velocity has only a slight effect on the pedal force. As the coil current changes from 0→1.1→0 A, the relationship curves between the pedal force and the coil current are gained in Figure 5(c). The two curves do not coincide with each other in the current increasing and decreasing stages. Specifically, the pedal force at the current decreasing stage is higher than that at the current increasing stage. We can infer that the pedal force generated by the MRDBBPS has an apparent hysteresis effect. The main reason is that MR fluids are composed of soft magnetic particles and other materials. In the process of repeated magnetization, the change of magnetic induction intensity of magnetic material always lags behind its magnetic field intensity, which will lead to the obvious hysteresis effect of pedal force. Moreover, the measured pedal force at a coil current of 1.1 A is 552 N, higher than the required value of 500 N, which means that the MRDBBPS prototype satisfies the force requirement.

3 Return-to-Zero Based Real-Time Current-Tracking Control Algorithm

3.1 Brake Pedal Characteristic Curve (BPCC)

Figure 6 depicts the relationship between the pedal force and pedal displacement, known as BPCC, for a CHB system in an A0-class car, which is obtained by testing the pedal characteristics of the hydraulic braking system of a passenger car [40]. In the figure, stage OA is for the elimination of the pedal clearance, during which the pedal force increases inconspicuously with the pedal displacement. However, the pedal force increases faster with the pedal displacement at stage AB because it acts on the vacuum booster. In stage BC, the pedal force acts directly on the brake cylinder and its value increases rapidly. In general, the pedal force increases non-linearly with the pedal displacement, and the increasing trend accelerates as the pedal displacement increases.

3.2 Return-to-Zero (RTZ) Algorithm

As Figure 5(c) shows, the pedal force exhibits an apparent hysteresis when the coil current is not 0. In other words, two pedal force values map to the same current value, which negatively affects the control accuracy. Figure 7 shows the change in the pedal force with the coil current in the range of 0→0.4→0→0.8→0→1.1→0 A. Generally, the pedal forces are equal without hysteresis when the current reduces to 0 from different values. Based on this feature, an RTZ algorithm is proposed to avoid the hysteresis of the pedal force.

The basic concept of the proposed RTZ algorithm is described as follows: when the driver steps on or maintains the pedal in an applied position, the pedal velocity $v \geq 0$, and a coil current is applied to the MR damper in accordance with the real-time pedal displacement. In contrast, if the driver releases the pedal, the pedal velocity $v < 0$, and an RTZ operation should be performed to the coil current. The algorithm can ensure that the coil current is applied from 0 every time the pedal is pressed to effectively avoid the hysteresis effect and improve the control accuracy and repeatability.

3.3 Real-Time Current-Tracking Algorithm

The RTZ algorithm requires the coil current to be capable of changing to the desired value in real-time. However, in practice, the response lag of the coil circuit also affects the real-time performance of the current

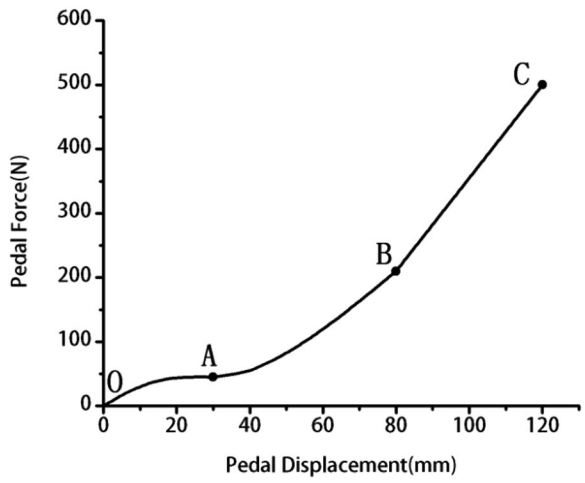

Figure 6 Relationship between the pedal force and pedal displacement for a CHB system

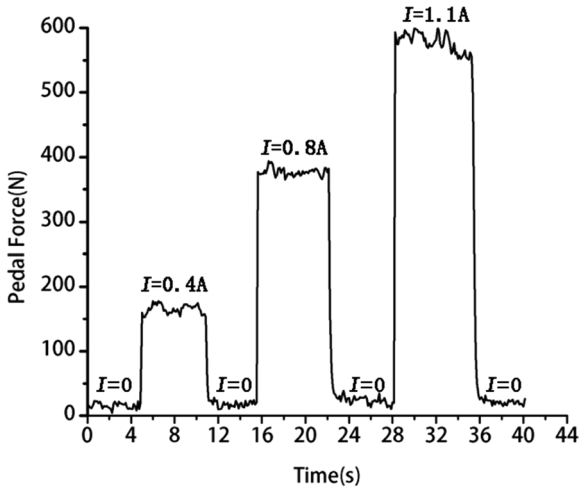

Figure 7 Changes in the pedal force once the coil current reduces to 0 from different values

output. Normally, the rheological time of MRFs is negligible, within a few milliseconds [41, 42]. While using a constant voltage source U as the power supply of the coil, the coil circuit can be equivalent to a series circuit composed of an inductor L and a resistor R. The following equation can be obtained

$$L \cdot \frac{\mathrm{d}I}{\mathrm{d}t} + R \cdot I = U. \tag{9}$$

Subsequently

$$I(t) = \frac{U}{R}(1 - e^{-\frac{t}{\tau}}), \tag{10}$$

where τ is the response time of the coil current, $\tau = \frac{L}{R}$. For the first-order inertial link, the response time refers to the time required for the current to attain 63.2% of its stable value. In this design, the response time is calculated as τ=90 ms according to the coil parameters. Since the brake pedal operates in a rapid movement state, a relatively large time delay negatively affects the accurate control of the coil current.

Therefore, a real-time current-tracking algorithm is proposed with its principle presented in Figure 8. At the initial moment, the current is I_0. When I_1 is applied, 5τ is required for the current to attain a stable value. However, the required time for the current to attain I_1 abruptly reduces to τ_1 when I_2 is applied. Since $\tau_1 \ll 5\tau$, a rapid response of the current is achieved, and the following equation can be obtained

$$(I_2 - I_0) \cdot (1 - e^{-\frac{\tau_1}{\tau}}) = I_1 - I_0. \tag{11}$$

Then

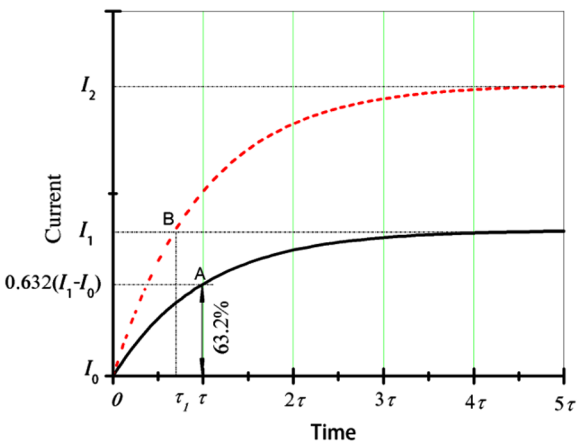

Figure 8 Principle of the real-time current-tracking algorithm

$$I_2 = \frac{I_1 - I_0}{1 - e^{-\frac{\tau_1}{\tau}}} + I_0. \tag{12}$$

Since the cycle of the pulse-width modulation (PWM) signal provided by the selected control card is 20 ms, the required time for the current to increase from I_0 to I_1 should be less than 20 ms. To avoid overshoot, the value of τ_1 is set as 20 ms.

Substituting the values of τ and τ_1 into Eq. (12) yields

$$I_2 = 5\Delta I + I_0, \tag{13}$$

where $\Delta I = I_1 - I_0$.

3.4 Controller Design

As shown in Figure 9, the controller is designed by considering the pedal displacement as the input and the duty ratio of the PWM signal as output. First, the equation of the relationship between the pedal force F and the pedal displacement s is fitted based on the BPCC in Figure 6. Subsequently, the relationship between the coil current I and the pedal force F is fitted by polynomial curve based on the least square method referring to the experimental data in Figure 5(c). During this step, the RTZ algorithm is integrated to determine whether the coil current must be reset to zero. Finally, because I is regulated by changing the duty ratio of the PWM signal d, the relationship between d and I is fitted accordingly.

Considering the hysteresis effect, the equation of the relationship between I and F can be adjusted by introducing the RTZ algorithm as follows:

$$\begin{aligned} I = \xi \cdot (&-0.0469 + 0.00343F - 5.13951 \\ &\times 10^{-6}F^2 + 4.89031 \times 10^{-9}F^3), \end{aligned} \tag{14}$$

where ξ is the coefficient of the RTZ algorithm. A pedal velocity of $v \geq 0$ means that the driver steps on or holds the pedal in the applied position, then ξ=1. If the pedal speed $v < 0$, it means the driver releases the pedal, then ξ=0.

$$\xi = \begin{cases} 1, & v \geq 0, \\ 0, & v < 0. \end{cases} \tag{15}$$

Figure 10 exhibits the block diagram of the RTZ algorithm-based real-time current-tracking controller (RTZRC). When the pedal is pressed, the encoder collects the values of s and v. If $v < 0$, the coil current returns to zero. Otherwise, the theoretical current I_1 is calculated with reference to Eq. (14), and it is transferred to the real-time current-tracking algorithm. Combining it with the initial current I_0 detected by the current sensor, the actual current I_2 and the duty ratio of the PWM signal d are calculated in turn. Finally, the corresponding

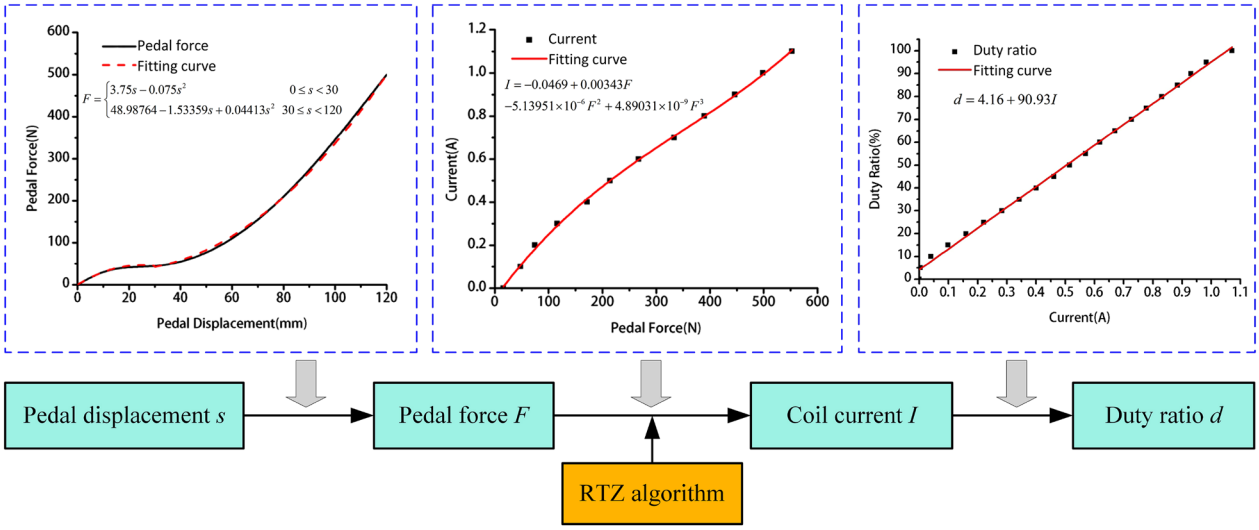

Figure 9 Design process of the controller

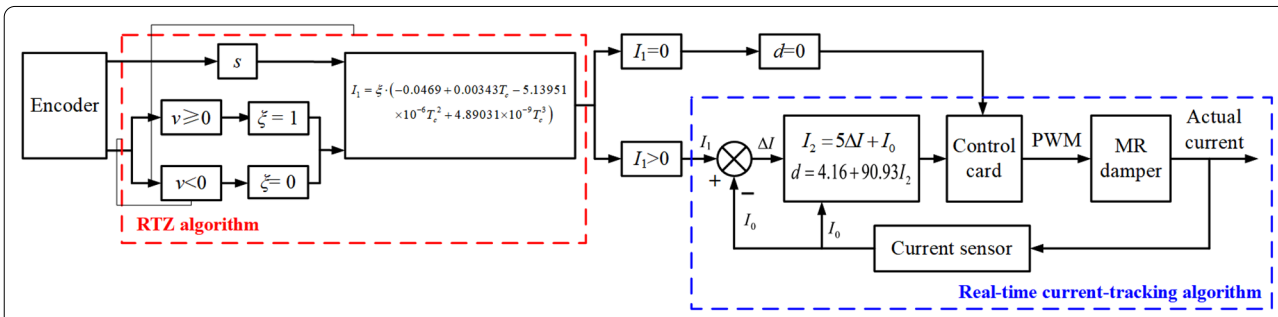

Figure 10 Block diagram of the RTZ algorithm-based real-time current-tracking controller (RTZRC)

coil current is supplied to the MR damper by the PWM signal, and the actual pedal force is measured by the pedal force sensor.

4 Experimental Evaluation

The following experiments are performed on the MRDBBPS prototype in combination with a self-developed automotive MR braking test bench (AMRBTB): 1) Tracking control experiments on the MRDBBPS prototype to evaluate the accuracy and effectiveness of the proposed control algorithm; 2) Braking experiments on the AMRBTB integrated with the MRDBBPS prototype to verify its actual control effect on the vehicle braking process.

4.1 Experimental System

The experimental system, shown physically in Figure 11, is established by integrating the MRDBBPS prototype into the self-developed AMRBTB. As shown in Figure 11(a), the entire system is primarily composed of three subsystems including the AMRBTB, a data acquisition and control system, and the MRDBBPS prototype. In more detail, the AMRBTB orienting to an A0-class quarter-car is developed using the single-ended inertial flywheel simulation mode. It primarily includes a motor, a flywheel set, a torque/speed sensor, an MR brake, as well as several couplings and supports. The main design parameters of the AMRBTB are listed in Table 1. For the data acquisition and control system shown in Figure 11(b), a main control card (model 74HC244) is used, which has a total of 16 input and output interfaces: 8 for analog-to-digital (AD) signal acquisition, 4 for counting, and 4 for the PWM signal output.

4.2 Control Experiments on the MRDBBPS Prototype

As mentioned above, to realize an accurate simulation of the BPCC is the key index to measure the performance of the MRDBBPS prototype and the proposed

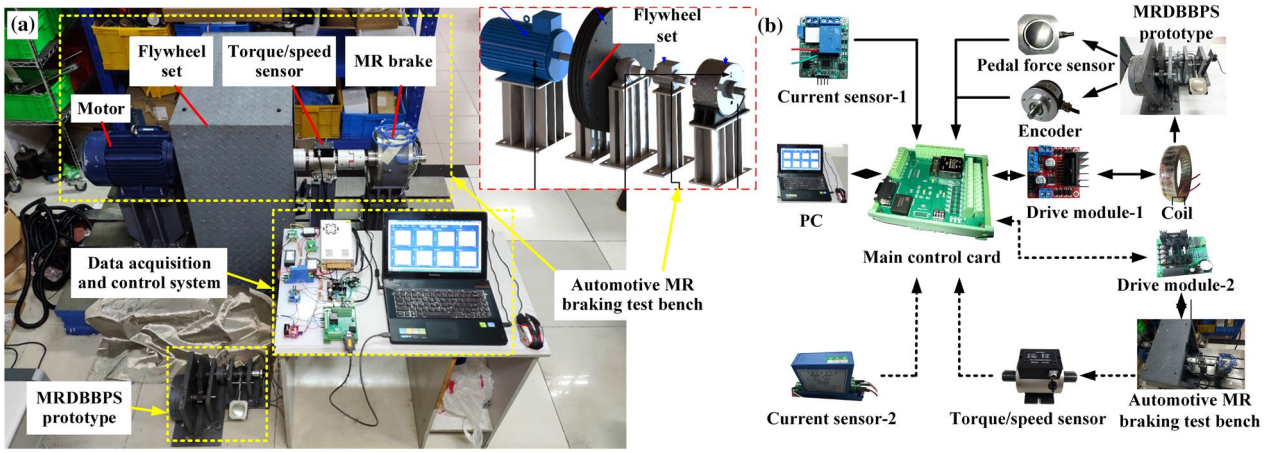

Figure 11 Experimental system: (**a**) Physical map, (**b**) data acquisition and control system

Table 1 Main design parameters of the AMRBTB

Design parameter		Value
Target vehicle	Full-load mass (kg)	1150
	Wheelbase (m)	2.34
	Distance between the gravity center and the front axle (m)	1.15
	Height of the gravity center when full-loaded (m)	0.55
	Rolling radius of the tire (m)	0.24
Flywheel	Diameter (m)	0.34
	Thickness (m)	0.02
	Mass (m)	55
Maximum braking torque of the MR brake (N·m)		240.3
Moment of inertia for the flywheel set (kg·m^2)		12.77
Motor model		Y132 M-4

control algorithm. Figure 12 exhibits a comparison of the BPCC tracking effect without and with the proposed control algorithm. To comprehensively assess the control performance under various conditions, the experiments are carried out at three levels of pedal velocity: low, medium, and high. The results indicate that the actual pedal force is apparently lower than the ideal pedal force, primarily because of the response lag of the coil induction circuit without the proposed control algorithm. The mean absolute error is used to evaluate the force tracking effect. The mean absolute error of force tracking at low, medium and high pedal velocity is 17.19 N, 19.90 N, 30.49 N without control algorithm respectively. As shown in Figure 12(b), with the help of the proposed control algorithm, the tracking effect turns much better, even at a high pedal velocity, and the mean absolute error of force tracking with control algorithm is 8.19 N, 8.90 N, 10.49 N. The

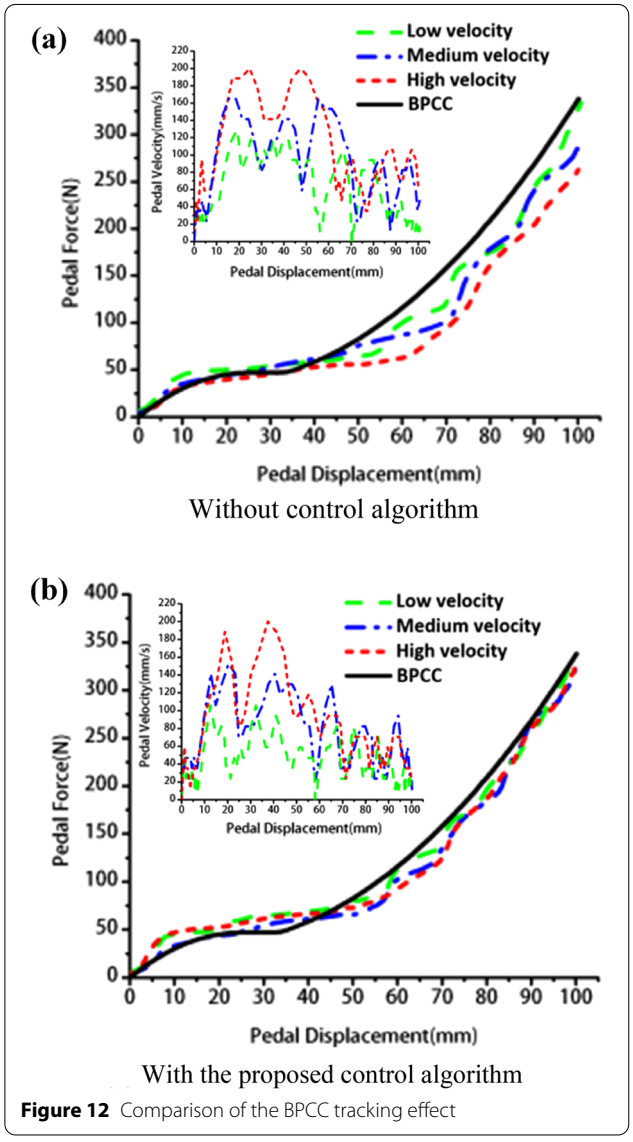

Figure 12 Comparison of the BPCC tracking effect

phenomenon in return verifies the effectiveness of the proposed control algorithm in Section III.

In order to further verify the effectiveness of the designed control algorithm, we have chosen the conventional PID algorithm for the pedal force tracking comparison experiment, and PID parameters are tuned based on the designer's experiences. As shown in Figure 13(a), comparing the experimental results of the three algorithms, both the PID algorithm and the proposed RTZRC algorithm have good tracking effects compared with the uncontrolled algorithm. However, an apparent hysteresis occurs without the control algorithm and the current difference becomes very large. As shown in Figure 13(b), When using RTZRC algorithm, the current is observed to approach the desired value, the current difference is maintained within 0.04 A and the mean absolute error of current difference is less than 0.016 A. The mean absolute error of current difference is slightly larger by PID algorithm, about 0.049 A. As a consequence, the RTZRC algorithm designed in this study has a good tracking effect on pedal force and coil current.

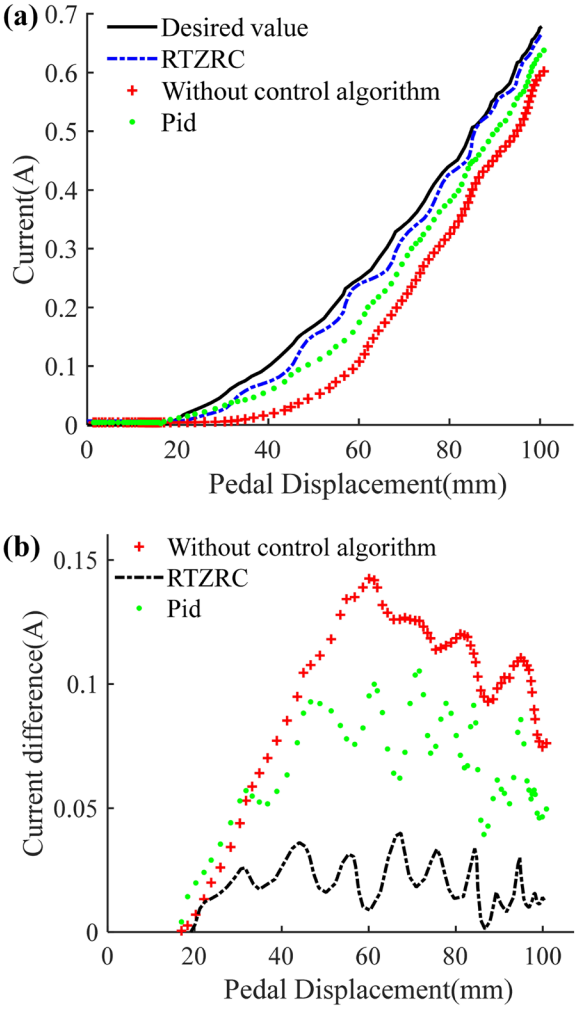

Figure 13 Effect of the proposed control algorithm on (**a**) current and (**b**) current difference

Figure 14 shows the variations in the pedal displacement, pedal force, and pedal velocity during the intermittent braking process. In the three experiments, labeled A, B and C, the pedal is initially pressed for different displacements, and then released, followed by a re-pressed again. The variation in the pedal force is observed to still satisfy a good tracking effect of the BPCC, and the results verifies the effectiveness of the RTZRC algorithm.

4.3 Braking Experiments on the AMRBTB

In this study, three groups of braking experiments with different intensities are conducted, including two emergency braking experiments (I and II), and a normal braking experiment (III). Figure 15 presents the changes in pedal displacement, velocity, and force under different braking intensities. The variation curves of the pedal parameters are observed to be basically consistent between experiments I and II, which indicates good repeatability for the MRDBBPS prototype. In addition, the maximum values of three pedal parameters in an emergency braking are greater than these in normal braking.

Figure 16 shows changes in the braking torque of the MR brake and vehicle speed during braking. Similarly, the changing curves under emergency braking I are

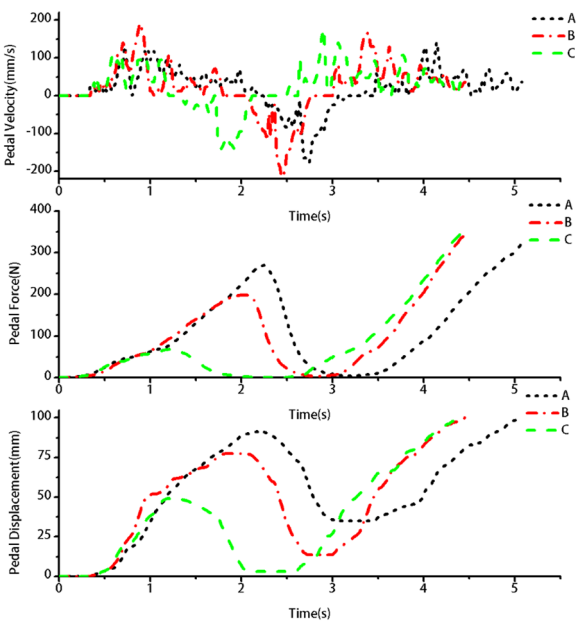

Figure 14 Variations in the pedal parameters during the intermittent braking process

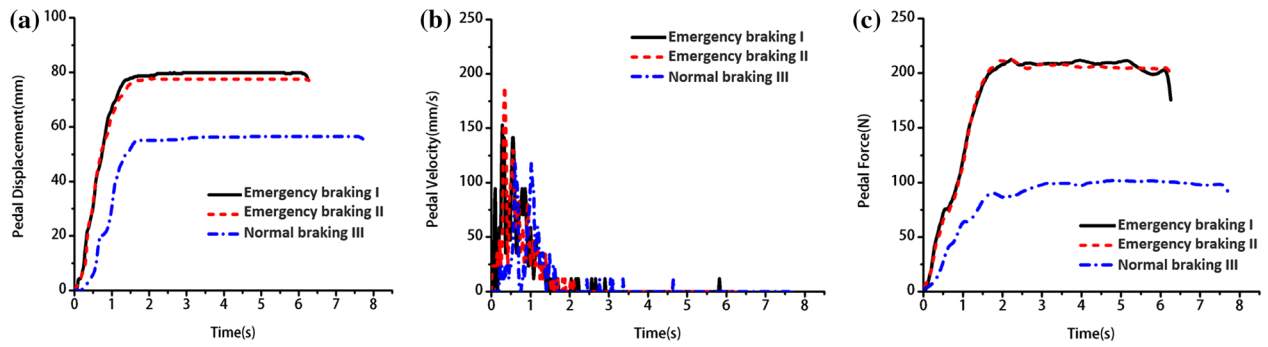

Figure 15 Variations in pedal parameters under different braking intensities: (**a**) Pedal displacement, (**b**) pedal velocity, (**c**) pedal force

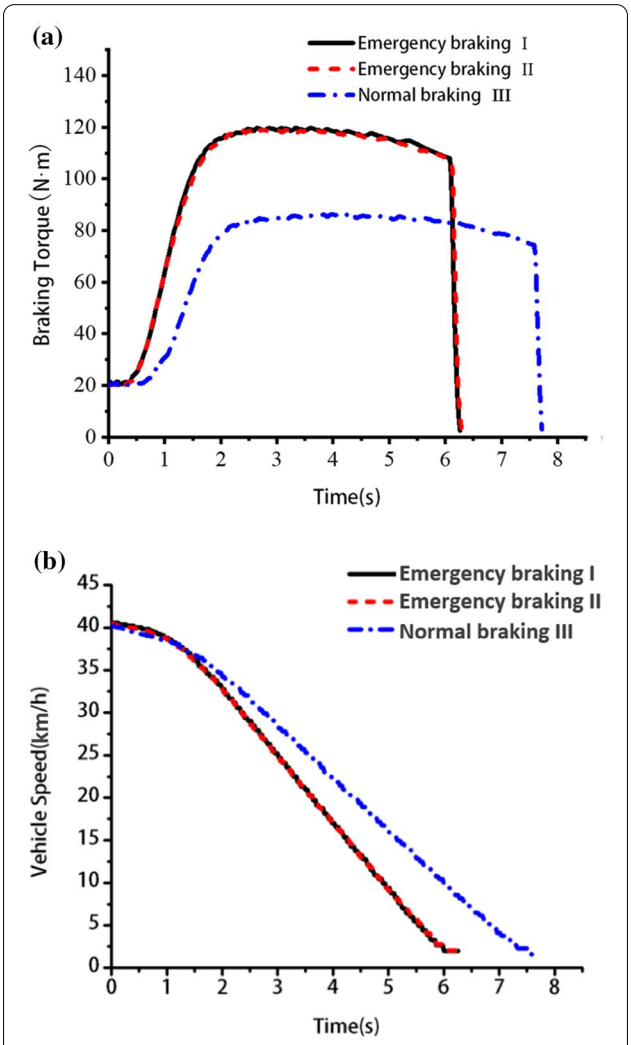

Figure 16 Changes in (**a**) the braking torque of the MR brake and (**b**) the vehicle speed during braking

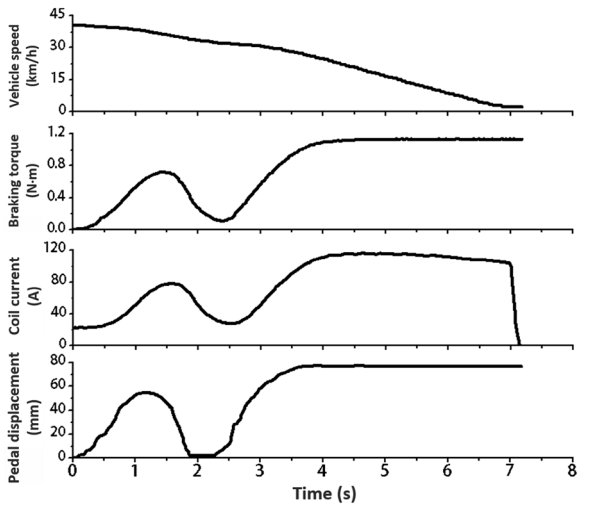

Figure 17 Braking parameter variations in the AMRBTB while stepping on the brake pedal

coincident with those under emergency braking II. The results indicate that the MRDBBPS prototype has a stable control effect on the AMRBTB under the same conditions. Moreover, the vehicle speed is observed to decline gradually under the action of the braking torque provided by the MR brake. For normal braking III, because of a small maximum pedal displacement, the braking torque is small, and the vehicle speed decreases gradually. The braking times are approximately 5.5 s and 6.8 s for the emergency and normal braking, respectively.

Figure 17 depicts the braking parameter variations of the AMRBTB while the brake pedal is pressed. As observed, the coil current, braking torque, and vehicle speed all change in accordance with the pedal displacement. For the first step on the brake pedal with a small

displacement, the vehicle speed declines gradually. After the brake pedal is released and re-pressed with a larger displacement, the declining trend of the vehicle speed becomes faster. The results verify that the MRDBBPS prototype achieves an effective and favorable control of the AMRBTB.

5 Conclusions

(1) In order to simulate the required BPF, a MRDBBPS based on the performance index is designed, which uses a compact disk-type MR damper to passively produce a controllable damping force under the excitation of a low-voltage direct current.
(2) The theoretical analysis and electromagnetic simulation of the designed MR damper are carried out, and several experiments on the pedal force characteristics of the MRDBBPS prototype are conducted. The results show that the maximum pedal force satisfies the design requirement.
(3) A real-time current tracking controller (RTZRC) based on RTZ algorithm is designed. By comparing the characteristic relationship between pedal displacement and pedal force, current and current difference under various algorithms, it is proved that RTZRC algorithm has good control performance and ensures the stability and accuracy of the relationship between pedal force and pedal displacement.
(4) The MRDBBPS prototype is integrated into the AMRBTB, and several control and braking experiments are conducted. Two groups of emergency braking experiments and one group of normal braking experiments are carried out to verify the stable control effect of the brake pedal sensation simulator on the brake test platform.
(5) Future studies are going to be executed regarding the structural optimization of the MRDBBPS and a more efficient control algorithm will be designed to achieve accurate real-time control of the relationship between pedal displacement and pedal force characteristics.

Acknowledgements
Not applicable.

Author's Contributions
DW was in charge of theoretical modelling, data analysis and manuscript writing; BW performed the experiments and prepared the draft; BZ and WC provided consultations and give suggestions on the manuscript writing; XB assisted with the control scheme formulation. All authors read and approved the final manuscript.

Authors' Information
Daoming Wang, born in 1987, is currently an associate professor at *School of Mechanical Engineering, Hefei University of Technology, China*. He received his PhD degree from *China University of Mining and Technology, China*, in 2014. His research interests include advanced braking system of vehicle, rehabilitation robots, and smart materials and structures.
Biao Wang, born in 1995, received his M.S. degree from *School of Mechanical Engineering, Hefei University of* Technology, *China*, in 2020. His research interests include vehicle brake-by-wire technology, smart materials and structures.
Bin Zi, born in 1975, is currently a professor and the dean of *School of Mechanical Engineering, Hefei University of Technology, China*. He received his PhD degree from *Xidian* University, *China*, in 2007. He has received the National Science Fund for Distinguished Young Scholars of China. His research interests include robotics and automation, and mechatronics. He is an Editorial Board Member of *Chinese Journal of Mechanical Engineering*, and *Mechanical Sciences*.
Xianxu Bai, born in 1984, is currently an associate professor at *School of Automobile and Transportation Engineering, Hefei University of Technology, China*. He received his PhD degree from *Chongqing University, China*, in 2013. His research interests include intelligent vehicle, smart structures and systems.
Wuwei Chen, born in 1951, is currently a professor at *School of Automobile and Transportation Engineering, Hefei University of Technology*, *China*. He received his PhD degree from *Anhui Institute of Optics and Fine Mechanics*, *Chinese Academy of Sciences*, *China*, in 1999. His research interests include intelligent vehicle, vehicle dynamics and control.

Funding
Supported by National Natural Science Foundation of China (Grant Nos. 52175047 and 51505114), and Anhui Provincial Natural Science Foundation of China (Grant No. 2008085ME140).

Competing interests
The authors declare no competing financial interests.

Author Details
[1]School of Mechanical Engineering, Hefei University of Technology, Hefei 230009, China. [2]School of Automobile and Transportation Engineering, Hefei University of Technology, Hefei 230009, China.

Received: 20 July 2021 Revised: 20 October 2022 Accepted: 26 October 2022
Published online: 18 November 2022

References

[1] Y Cai, H Wang, X Chen, et al. Vehicle detection based on visual saliency and deep sparse convolution hierarchical model. *Chinese Journal of Mechanical Engineering*, 2016, 29(4): 765–772.
[2] X Wang, X Wu, S Cheng, et al. Design and experiment of control architecture and adaptive dual-loop controller for brake-by-wire system with an electric booster. *IEEE Transactions on Transportation Electrification*, 2020, 6(3): 1236-1252.
[3] L Zhang, Z Zhang, Z Wang, et al. Chassis coordinated control for full x-by-wire vehicles-a review. *Chinese Journal of Mechanical Engineering*, 2021, 34(1). https://doi.org/10.1186/s10033-021-00555-6.
[4] S Huang, C Zhou, L Yang, et al. Transient fault tolerant control for vehicle brake-by-wire systems. *Reliability Engineering and System Safety*, 2016, 149: 148-163.
[5] M R A Atia, S A Haggag, A M M Kamal. Enhanced electromechanical brake-by-wire system using sliding mode controller. *Journal of Dynamic Systems, Measurement, and Control-Transactions of the ASME*, 2016, 138(4): 1003-1029.
[6] S A Haggag, D Abidou. An approach to vehicle brake-by-wire optimal control tracking strategy. *SAE International Journal of Passenger Cars - Mechanical Systems*, 2013, 6(2013): 154-162.
[7] D Meng, L Zhang, Z Yu. A dynamic model for brake pedal feel analysis in passenger cars. *Proceedings of the Institution of Mechanical Engineers, Part D: Journal of Automobile Engineering*, 2016, 230(7): 955-968.

[8] Y Aoki, K Suzuki, H Nakano, et al. Development of hydraulic servo brake system for cooperative control with regenerative brake. *SAE Technical Paper*, 2007.
[9] J W Zehnder, S S Kanetkar, C A Osterday. Variable rate pedal feel emulator designs for a brake-by-wire system. *SAE Transactions*, 1999: 881-884.
[10] Y Liu, Z Sun, J I Wenbin. Development of composite brake pedal stroke simulator for electro-hydraulic braking system. *SAE Technical Paper*, 2014.
[11] Y L Yu, Y H Xu, Y N Xu. Research of sensor fault-tolerant control based on analytical reconstruction model for electronic brake pedal simulator. *International Journal of Modeling and Optimization*, 2015, 5(6): 361-365.
[12] M Flad, S Rothfuss, G Diehm, et al. Active brake pedal feedback simulator based on electric drive. *SAE International Journal of Passenger Cars-Electronic and Electrical Systems*, 2014, 7(1): 189-200.
[13] E Farshizadeh, D Steinmann, H Briese, et al. A concept for an electrohydraulic brake system with adaptive brake pedal feedback. *Proceedings of the Institution of Mechanical Engineers, Part D: Journal of Automobile Engineering*, 2015, 229(6): 708-718.
[14] A Hildebrandt, O Sawodny, R Trutschel, et al. Nonlinear control design for implementation of specific pedal feeling in brake-by-wire car design concepts. *Proceeding of the 2004 American Control Conference*, 2004, 2(1): 1463-1468.
[15] D Wang, B Zi, S Qian, et al. Steady-state heat-flow coupling field of a high-power magnetorheological fluid clutch utilizing liquid cooling. *Journal of Fluids Engineering-Transactions of the ASME*, 2017, 139(11) : 1105-1116.
[16] S H Mousavi, H Sayyaadi. Optimization and testing of a new prototype hybrid MR brake with arc form surface as a prosthetic knee. *IEEE/ASME Transactions on Mechatronics*, 2018, 23(3): 1204-1214.
[17] P Zhang, K H Lee, C H Lee. Friction behavior of magnetorheological fluids with different material types and magnetic field strength. *Chinese Journal of Mechanical Engineering*, 2016, 29(1): 84-90.
[18] M Moghani, M R Kermani. A lightweight magnetorheological actuator using hybrid magnetization. *IEEE/ASME Transactions on Mechatronics*, 2019, 25(1): 76-83.
[19] M K Thakur, C Sarkar. Influence of graphite flakes on the strength of magnetorheological fluids at high temperature and its rheology. *IEEE Transactions on Magnetics*, 2020, 56(5): 1-10.
[20] X Tang, H Du, S Sun, et al. Takagi–Sugeno fuzzy control for semi-active vehicle suspension with a magnetorheological damper and experimental validation. *IEEE/ASME Transactions on Mechatronics*, 2016, 22(1): 291-300.
[21] R Jeyasenthil, S B Choi. A novel semi-active control strategy based on the quantitative feedback theory for a vehicle suspension system with magneto-rheological damper saturation. *Mechatronics*, 2018, 54: 36-51.
[22] S Sun, X Tang, J Yang, et al. A new generation of magnetorheological vehicle suspension system with tunable stiffness and damping characteristics. *IEEE Transactions on Industrial Informatics*, 2019, 15(8): 4696-4708.
[23] X Bai, S Shen, N M Wereley, et al. Controllability of magnetorheological shock absorber: I. Insights, modeling and simulation. *Smart Materials and Structures*, 2018, 28(1): 5022-5066.
[24] Q Ouyang, H Hu, C Qian, et al. Investigation of the influence of magnetic field distribution on the magnetorheological absorber with individually controllable coils. *IEEE Transactions on Magnetics*, 2019, 55(8): 1-13.
[25] D Wang, B Zi, Y Zeng, et al. Simulation and experiment on transient temperature field of a magnetorheological clutch for vehicle application. *Smart Materials and Structures*, 2017, 26(9): 095020.
[26] S R Patil, K P Powar, S M Sawant. Thermal analysis of magnetorheological brake for automotive application. *Applied Thermal Engineering*, 2016, 98: 238-245.
[27] L Yu, L Ma, J Song, et al. Magnetorheological and wedge mechanism-based brake-by-wire system with self-energizing and self-powered capability by brake energy harvesting. *IEEE/ASME Transactions on Mechatronics*, 2015, 21(5): 2568-2580.
[28] D Wang, Y Wang, Z Cao, et al. Development of an active and passive finger rehabilitation robot using pneumatic muscle and magnetorheological damper. *Mechanism and Machine Theory*, 2020, 147(2020): 3762-3778.
[29] T Oba, H Kadone, M Hassan, et al. Robotic ankle-foot orthosis with a variable viscosity link using MR fluid. *IEEE/ASME Transactions on Mechatronics*, 2019, 24(2): 495-504.
[30] D Wang, Y Wang, J Pang, et al. Development and control of an MR brake-based passive force feedback data glove. *IEEE Access*, 2019, 7: 172477-172488.
[31] D Chen, A Song, L Tian, et al. Development of a multidirectional controlled small-scale spherical MR actuator for haptic applications. *IEEE/ASME Transactions on Mechatronics*, 2019, 24(4): 1597-1607.
[32] Y Song, S Guo, X Yin, et al. Design and performance evaluation of a haptic interface based on MR fluids for endovascular tele-surgery. *Microsystem Technologies*, 2018, 24(2): 909-918.
[33] T H Yang, H Son, S Byeon, et al. Magnetorheological fluid haptic shoes for walking in VR. *IEEE Transactions on Haptics*, 2020, 14(1): 83-94.
[34] A J Day, H P Ho, K Hussain, et al. Brake system simulation to predict brake pedal feel in a passenger car. *SAE Technical Paper*, 2009.
[35] D Aleksendric, V Cirovic, D Smiljanic. Brake pedal feel control model. *SAE Technical Paper*, 2015.
[36] K Yan, X Tang, Y Qin, et al. Comparative study of trajectory tracking control for automated vehicles via model predictive control and robust H-infinity state feedback control. *Chinese Journal of Mechanical Engineering*, 2021, 34(1): 1-14.
[37] L Zhang, C Ruan, D Meng. The influence of vacuum booster design parameters on brake pedal feel. *SAE International Journal of Passenger Cars - Mechanical Systems*, 2014, 7(8): 1311-1320.
[38] X Tang, Z Zhang, Y Qin. On-road object detection and tracking based on radar and vision fusion: A review. *IEEE Intelligent Transportation Systems Magazine*, 2021: 2-27.
[39] D Wang, Y Hou, Z Tian. A novel high-torque magnetorheological brake with a water cooling method for heat dissipation. *Smart Materials and Structures*, 2013, 22(2): 5019-5030.
[40] F Ji, X Zhou, W Zhu. Pedal simulator and braking feel evaluation in brake by wire system. *Journal of Beijing University of Aeronautics and Astronautics*, 2015, 41(6): 989-994.
[41] Y Chen, M Zhou, L Geng, et al. Transmission impedance extraction method applied in magneto-rheological damper. *International Journal of Applied Electromagnetics and Mechanics*, 2018, 56(2): 317-327.
[42] K Dai, Y Liu, M Okui, et al. Variable viscoelasticity handshake manipulator for physical human-robot interaction using artificial muscle and MR brake. *Smart Materials and Structures*, 2019, 28(6): 4002-4013.